Decoherence of Bell states by local interactions with a suddenly quenched spin environment

Pierre Wendenbaum,[1,2] Bruno G. Taketani,[2] and Dragi Karevski[1,*]

[1]*Institut Jean Lamour, dpt P2M, Groupe de Physique Statistique, Université de Lorraine-CNRS, B.P. 70239, F-54506 Vandœuvre-lès-Nancy Cedex, France*

[2]*Theoretische Physik, Universität des Saarlandes, D-66123 Saarbrücken, Germany*

(Received 26 May 2014; published 29 August 2014)

We study the dynamics of disentanglement of two qubits initially prepared in a Bell state and coupled at different sites to an Ising spin chain in a transverse field (ITF) playing the role of a dynamic spin environment. The initial state of the whole system is prepared in a tensor product state $\rho_{\text{Bell}} \otimes \rho_{\text{chain}}$, where the state of the chain is taken to be given by the ground state $|G(\lambda_i)\rangle$ of the ITF Hamiltonian $H_E(\lambda_i)$ with an initial field λ_i. At time $t = 0^+$, the strength of the transverse field is suddenly quenched to a new value, λ_f, and the whole system (chain + qubits) undergoes a unitary dynamics generated by the total Hamiltonian $H_{\text{Tot}} = H_E(\lambda_f) + H_I$, where H_I describes a local interaction between the qubits and the spin chain. The resulting dynamics leads to a disentanglement of the qubits, which is described through Wootters' concurrence, due to their interaction with the nonequilibrium environment. The concurrence is related to the Loschmidt echo, which in turn is expressed in terms of the time-dependent covariance matrix associated with the ITF. This permits a precise numerical and analytical analysis of the disentanglement dynamics of the qubits as a function of their distance, bath properties, and quench amplitude. In particular, we emphasize the special role played by a critical initial environment.

DOI: 10.1103/PhysRevA.90.022125 PACS number(s): 03.65.Yz, 03.67.Bg, 03.67.Mn

I. INTRODUCTION

Entanglement is one of the most intriguing features of nature [1] predicted by quantum mechanics. Since the pioneering discussion by Einstein, Podolsky and Rosen in there celebrated paper [2], the dramatic consequences of quantum entanglement have been extensively studied on both theoretical and experimental sides (see [3] for an historical review). If these initial studies were first orientated to a better understanding of the foundations of quantum mechanics, more recent investigations on entanglement phenomena focused on potential technological applications such as quantum computing [4] and quantum simulation [5].

However, entanglement is generally very sensitive to decoherence generated by the unavoidable interactions with the system's environment [6–8], responsible for the loss of the typical quantum features one wishes to exploit. It is consequently of primary importance to understand these decoherence processes in order to suppress or possibly exploit it. For example, in order to limit the decoherence process, dynamical control consisting in pulses applied to the system has been proposed in [9,10]. Engineered non-equilibrium dynamics have also been suggested to create entangled steady-states [11,12] and to assist precision measurements [13]. From a different perspective, typical quantum information tools such as entanglement have been applied in many-body systems to identify signatures of quantum phase transitions [14] and to characterize the ground state close to a critical point [15].

Aiming at a better understanding of decoherence, a number of models have investigated the dynamics of a small system interacting with a given typical environment. Among them one may mention the central spin model, where the system made of one or two spins is simultaneously coupled to many interacting spins [16–24]. Particular focus has been on critical spin environments which were shown to lead to enhanced decoherence [17] and to universal properties [18]. Cormick and Paz [25] went beyond the standard central spin system and studied the dependence of decoherence on the spatial separation of two qubits, initially prepared in a Bell state, when they interact locally with an extended equilibrium environment modeled by a quantum spin-1/2 chain in a transverse field. They found, in particular, that in the strong-coupling limit decoherence typically increases with the qubit separation distance and, finally, saturates when the qubit separation is over a threshold distance related to the spin chain correlation length.

In this work, we extend the work of Cormick and Paz [25] by considering an environment which is set out of equilibrium by a sudden change in a global environment coupling constant, the so-called global quantum quench [26,27]. Quantum quench protocols have received much attention in recent years, for example, in the context of the quantum version of fluctuation theorem [28] and relaxation properties toward a local canonical ensemble or a generalized version of the Gibbs ensemble depending on the integrability of the system (see [27] for a review). Many of these investigations focus not only on steady properties but also on dynamical aspects like front propagation of an initial density inhomogeneity [29–32] or expansion of a cloud of particles after the more or less sudden release of a trap [33–36]. Our main goal here is to investigate how the quench—that is, how the relaxation of the environment toward a local steady state [27]—influences, with respect to the equilibrium case treated in [25], the disentanglement of the two distant qubits initially prepared in a Bell state.

The paper is organized as follows: In Sec. II we present the model describing two qubits coupled to an Ising chain in a transverse field (ITF). In Sec. III the dynamics is diagonalized through the Jordan-Wigner representation of the ITF and an explicit relation is given for the Loschmidt echo through the time evolution of the two-point correlation functions of the ITF. Section IV is devoted to the quench behavior of

*dragi.karevski@univ-lorraine.fr

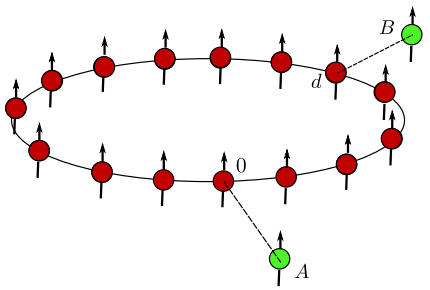

FIG. 1. (Color online) Two defect spins (qubits), A and B, are locally coupled to a spin chain.

the disentanglement of the qubits studied numerically and analytically. Finally, in Sec. V we draw our conclusions.

II. THE MODEL AND THE ENTANGLEMENT MEASURE

A. Two qubits coupled to an Ising chain

We consider in the following two noninteracting qubits coupled locally to an Ising quantum chain with N spins (see Fig. 1). The total Hamiltonian (qubits + chain) governing the dynamics of the whole system is given by

$$H_{\rm Tot} = H_E + H_I, \tag{1}$$

where H_E is the Ising chain (environment) Hamiltonian

$$H_E(\lambda) = -J\sum_{j=0}^{N-1}\sigma_j^x\sigma_{j+1}^x - \lambda\sum_{j=0}^{N-1}\sigma_j^z, \tag{2}$$

where the σ's are the usual Pauli matrices. The nearest-neighbor coupling J is taken to be positive and λ is a transverse field. We work with periodic boundary conditions, i.e., $\sigma_N^i = \sigma_0^i$, with $i = x,y,z$. The interaction Hamiltonian describing the coupling of the qubits, labeled A and B, at different sites of the chain separated by a distance d is given by

$$H_I = -\varepsilon\left(|\uparrow\rangle\langle\uparrow|_A\otimes\sigma_0^z + |\uparrow\rangle\langle\uparrow|_B\otimes\sigma_d^z\right), \tag{3}$$

where $|\uparrow\rangle_{A,B}$ is an eigenstate of $\sigma_{A,B}^z$ satisfying $\sigma_{A,B}^z|\uparrow\rangle_{A,B} = |\uparrow\rangle_{A,B}$ and $\varepsilon > 0$ sets the intensity of that interaction.

The two qubits are assumed to be initially in the maximally entangled Bell state $|\phi\rangle_{AB} = \frac{1}{\sqrt{2}}(|\uparrow\uparrow\rangle + |\downarrow\downarrow\rangle)$ and uncorrelated with the bath, such that the initial state of the total system is a tensor state $|\psi(0)\rangle = |\phi\rangle_{AB}\otimes|G(\lambda_i)\rangle_E$, with $|G(\lambda_i)\rangle_E$ the ground state of the initial bath Hamiltonian $H_E(\lambda_i)$.

At time $t = 0^+$ the transverse field of the Ising chain is suddenly quenched to a new value λ_f, forcing the system to evolve in a nonequilibrium regime. Due to the structure of the interaction Hamiltonian and the initial state, the total dynamics splits into two different channels, each governed by a specific Hamiltonian, namely, $H_{\downarrow\downarrow}(\lambda_f) = H_E(\lambda_f)$ if the two qubits are in state $|\downarrow\downarrow\rangle$ and $H_{\uparrow\uparrow}(\lambda_f) = H_E(\lambda_f) - \varepsilon(\sigma_0^z + \sigma_d^z)$ if they are in state $|\uparrow\uparrow\rangle$. Note here that $H_{\uparrow\uparrow}$ has exactly the same structure as H_E, the only difference being that the transverse fields acting at sites 0 and d are changed to the value $\lambda+\varepsilon$ instead of λ. Consequently, the time evolution of the initial state $|\psi(0)\rangle = |\phi\rangle_{AB}\otimes|G(\lambda_i)\rangle$ is given by

$$|\psi(t)\rangle = \frac{1}{\sqrt{2}}[|\uparrow\uparrow\rangle\otimes|\varphi_{\uparrow\uparrow}(t)\rangle_E + |\downarrow\downarrow\rangle\otimes|\varphi_{\downarrow\downarrow}(t)\rangle_E], \tag{4}$$

with the evolved states

$$|\varphi_\alpha(t)\rangle_E = e^{-iH_\alpha(\lambda_f)t}|G(\lambda_i)\rangle_E, \tag{5}$$

where $\alpha = \uparrow\uparrow,\downarrow\downarrow$.

The reduced density matrix of the qubits, $\rho_s(t) = {\rm Tr}_E\{|\psi(t)\rangle\langle\psi(t)|\}$, is given in the computational base $\{|\uparrow\uparrow\rangle,|\uparrow\downarrow\rangle,|\downarrow\uparrow\rangle,|\downarrow\downarrow\rangle\}$ by

$$\rho_s(t) = \frac{1}{2}\begin{pmatrix} 1 & 0 & 0 & D_{\uparrow\uparrow,\downarrow\downarrow}(t)\\ 0 & 0 & 0 & 0\\ 0 & 0 & 0 & 0\\ D^*_{\uparrow\uparrow,\downarrow\downarrow}(t) & 0 & 0 & 1\end{pmatrix}, \tag{6}$$

where the decoherence factor $D_{\uparrow\uparrow,\downarrow\downarrow}(t) = \langle\varphi_{\downarrow\downarrow}(t)|\varphi_{\uparrow\uparrow}(t)\rangle$ is explicitly given by

$$D_{\uparrow\uparrow,\downarrow\downarrow}(t) = \langle G(\lambda_i)|e^{iH_{\downarrow\downarrow}(\lambda_f)t}e^{-iH_{\uparrow\uparrow}(\lambda_f)t}|G(\lambda_i)\rangle. \tag{7}$$

Since the populations of the two defect spins do not change in time we see here that our model describes in the computational base a purely dephasing dynamics.

The decoherence factor D, governing the dynamics of the qubits, is simply related to the so-called Loschmidt echo [37] via

$$\mathcal{L}_{\uparrow\uparrow,\downarrow\downarrow}(t) = |\langle G(\lambda_i)|e^{iH_{\downarrow\downarrow}(\lambda_f)t}e^{-iH_{\uparrow\uparrow}(\lambda_f)t}|G(\lambda_i)\rangle|^2. \tag{8}$$

Note that if the final magnetic field is equal to the initial one ($\lambda_i = \lambda_f$, meaning that the bath is not quenched), the initial state $|G(\lambda_i)\rangle$ is the ground state of the Hamiltonian $H_{\downarrow\downarrow}(\lambda_i)$ and the echo is reduced to $\mathcal{L}(t) = |\langle G(\lambda_i)|e^{-iH_{\uparrow\uparrow}(\lambda_i)t}|G(\lambda_i)\rangle|^2$, which is the case treated in [25].

B. Entanglement measure

We use Wootters' concurrence [38,39] as the entanglement measure of our qubit system since in this case it takes a very simple form. For a two-qubit system the concurrence associated with state ρ is given by

$$\mathcal{C}(\rho) = \max\{0,\varepsilon_1 - \varepsilon_2 - \varepsilon_3 - \varepsilon_4\}, \tag{9}$$

where the ε_i's are the square roots of the eigenvalues in decreasing order of the (generally) non-Hermitian matrix $R = \rho\tilde{\rho}$, with $\tilde{\rho}$ defined as

$$\tilde{\rho} = (\sigma_y\otimes\sigma_y)\rho^*(\sigma_y\otimes\sigma_y), \tag{10}$$

where the complex conjugation is taken in the computational base. For the density matrix (6) the matrix $\tilde{\rho} = \rho$ and then

$$R = \rho^2 = \frac{1}{4}\begin{pmatrix} 1+|D|^2 & 0 & 0 & 2D\\ 0 & 0 & 0 & 0\\ 0 & 0 & 0 & 0\\ 2D^* & 0 & 0 & 1+|D|^2\end{pmatrix}, \tag{11}$$

which leads, for the eigenvalues, to $\varepsilon_1 = \frac{1}{4}(1+|D|)^2$, $\varepsilon_2 = \frac{1}{4}(1-|D|)^2$, and $\varepsilon_3 = \varepsilon_4 = 0$. Finally, for state (6) the

concurrence is simply given by

$$\mathcal{C}_{AB}(t) = \sqrt{\mathcal{L}(t)} = |D(t)|. \tag{12}$$

The entire dynamics of the two qubits A and B is encoded in the Loschmidt echo and the main goal of this study is to determine it.

III. LOSCHMIDT ECHO IN THE FERMIONIC REPRESENTATION

A. Jordan-Wigner transformation

The dynamics of the qubit system is generated through the two environment channels described by $H_{\uparrow\uparrow}$ and $H_{\downarrow\downarrow}$, which, as stated before, have the same structure except for two defect transverse fields, at positions 0 and d. Apart from that, these Hamiltonians are both diagonalized through the same standard procedure, that is, performing a Jordan-Wigner mapping followed by a Bogoliubov transformation, and in the following we drop the indices $\uparrow\uparrow$ and $\downarrow\downarrow$. In terms of the ladder operators $\sigma^{\pm} = \frac{\sigma^x \pm i\sigma^y}{2}$ the Jordan-Wigner mapping reads

$$\sigma_j^+ = e^{i\pi \sum_{i=0}^{j-1} c_i^\dagger c_i} c_j^\dagger, \quad \sigma_j^- = c_j e^{-i\pi \sum_{i=0}^{j-1} c_i^\dagger c_i}, \tag{13}$$

where the operators c_j and $c_j^\dagger$ satisfy the canonical Fermi algebra $\{c_i, c_j^\dagger\} = \delta_{i,j}$ and $\{c_i, c_j\} = \{c_i^\dagger, c_j^\dagger\} = 0$. In terms of the Fermi algebra the environmental Hamiltonians in the relevant parity sector become

$$H = \sum_{i,j} \left(c_i^\dagger A_{ij} c_j + \frac{1}{2}(c_i^\dagger B_{ij} c_j^\dagger + \text{H.c.}) \right), \tag{14}$$

with $A_{ij} = -2\lambda_i \delta_{ij} - J[\delta_{i,j-1} + \delta_{i,j-1}]$ and $B_{ij} = J[\delta_{i,j+1} - \delta_{i,j-1}]$ (indices N are identified with 0 to account for the periodic boundaries), defining, respectively, $N \times N$ symmetric and antisymmetric matrices A and B. Introducing the field operator

$$\mathbf{\Psi}^\dagger = (\boldsymbol{C}, \boldsymbol{C}^\dagger) = (c_0, \ldots, c_{N-1}, c_0^\dagger, \ldots, c_{N-1}^\dagger), \tag{15}$$

the Hamiltonian is further rewritten in a more compact form,

$$H = \tfrac{1}{2} \mathbf{\Psi}^\dagger \mathcal{H} \mathbf{\Psi}, \tag{16}$$

with the single-particle Hamiltonian

$$\mathcal{H} = \begin{pmatrix} -A & -B \\ B & A \end{pmatrix}. \tag{17}$$

In order to diagonalize the Hamiltonian H we introduce the unitary matrix

$$U = \begin{pmatrix} g & h \\ h & g \end{pmatrix} \tag{18}$$

that diagonalizes the single-particle matrix $\mathcal{H}$: $\Lambda = U^\dagger \mathcal{H} U$. The Hamiltonian H is readily diagonalized in terms of normal modes $\boldsymbol{\eta} = U^\dagger \mathbf{\Psi}$ and takes the form

$$H = \tfrac{1}{2} \boldsymbol{\eta}^\dagger \Lambda \boldsymbol{\eta}. \tag{19}$$

More explicitly, the normal mode operators $\boldsymbol{\eta}^\dagger = (\eta_0, \ldots, \eta_{N-1}, \eta_0^\dagger, \ldots, \eta_{N-1}^\dagger)$ are related to the original Fermi operators by the real Bogoliubov coefficients g_{ij} and h_{ij} through

$$\eta_k = \sum_i (g_{ik} c_i + h_{ik} c_i^\dagger) \tag{20}$$

and similar expressions for the adjoints $\eta_k^\dagger$. These relations are easily inverted and lead to

$$c_i = \sum_k (g_{ik} \eta_k + h_{ik} \eta_k^\dagger) \tag{21}$$

for the original Fermi operators in terms of the normal mode operators.

B. Time evolution of the covariance mat rix and Loschmidt echo

Since the Hamiltonians H_α with $\alpha = \uparrow\uparrow, \downarrow\downarrow$ are free fermionic, the Loschmidt echo, (8), describing the overlap between the states $|\varphi_\alpha(t)\rangle = e^{-iH_\alpha t}|G(\lambda_i)\rangle$, can be expressed in terms of the covariance matrices

$$C_\alpha(t) = \langle \varphi_\alpha(t) | \mathbf{\Psi} \mathbf{\Psi}^\dagger | \varphi_\alpha(t) \rangle \tag{22}$$

only and reads [40]

$$\mathcal{L}_{\uparrow\uparrow,\downarrow\downarrow}(t) = |\det(\mathbb{1} - C_{\downarrow\downarrow}(t) - C_{\uparrow\uparrow}(t))|^{1/2}, \tag{23}$$

where $\mathbb{1}$ is the $2N \times 2N$ identity matrix. The problem of computing the Loschmidt echo is then related to the evaluation of the time-evolved covariance matrices $C_\alpha(t)$. In order to derive this time dependence it is more convenient to switch to the Heisenberg picture. Thanks to the quadratic structure of the Hamiltonians H_α, the equations of motion for the field operators $\mathbf{\Psi}_\alpha$ in each channel $\alpha = \uparrow\uparrow, \downarrow\downarrow$ take the form

$$i \frac{d}{dt} \mathbf{\Psi}_\alpha = \mathcal{H}_\alpha \mathbf{\Psi}_\alpha, \tag{24}$$

where $\mathcal{H}_\alpha$ is the single-particle Hamiltonian, (17), associated with channel α. Together with the initial conditions $\mathbf{\Psi}_\alpha(0) = \mathbf{\Psi}$, these equations of motion are easily integrated and lead to $\mathbf{\Psi}_\alpha(t) = e^{-it\mathcal{H}_\alpha} \mathbf{\Psi}$. This allows us to write the time evolution of the covariance matrix as

$$C_\alpha(t) = e^{-it\mathcal{H}_\alpha} C(0) e^{it\mathcal{H}_\alpha}, \tag{25}$$

with $C(0) = \langle G(\lambda_i) | \mathbf{\Psi} \mathbf{\Psi}^\dagger | G(\lambda_i) \rangle$ the initial covariance matrix. In terms of the field operators $\boldsymbol{C}$ and $\boldsymbol{C}^\dagger$ it is given by

$$C(0) = \begin{pmatrix} \langle \boldsymbol{C}^\dagger \boldsymbol{C} \rangle & \langle \boldsymbol{C}^\dagger \boldsymbol{C}^\dagger \rangle \\ \langle \boldsymbol{C} \boldsymbol{C} \rangle & \langle \boldsymbol{C} \boldsymbol{C}^\dagger \rangle \end{pmatrix}, \tag{26}$$

where $\langle . \rangle$ is the operator's expectation value in the ground state $|G(\lambda_i)\rangle$. Consequently, the Loschmidt echo, (23), is explicitly derived from (25) given the initial covariance matrix $C(0)$.

IV. QUENCH DYNAMICS

A. Weak and strong coupling regimes

Let us consider first the influence of the coupling strength ε on the decoherence dynamics of the qubits for a given quench protocol. In Fig. 2 we have plotted the time evolution of the Loschmidt echo as a function of ε for an initial field $\lambda_i = 1.5$ and quenched at $\lambda_f = 0.5$. One sees that at a given quench

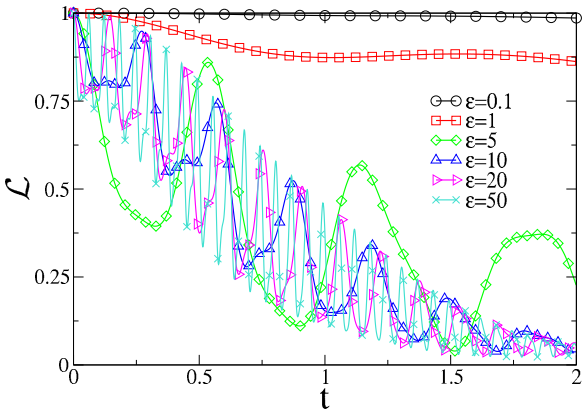

FIG. 2. (Color online) Time evolution of the Loschmidt echo after a quench from $\lambda_i = 1.5$ to $\lambda_f = 0.5$ for several coupling strengths ε. The distance is fixed at $d = 1$ and the size of the environment is $N = 100$.

protocol the decoherence is faster when the coupling strength is increased. Whereas the echo decreases slowly for weak coupling, $\varepsilon \ll 1$, the behavior is quite different in the strong coupling regime, $\varepsilon \gg 1$. Indeed, one observes fast oscillations of the echo $\mathcal{L}$ which are embedded inside an envelope that is independent of the coupling strength at sufficiently large ε ($\varepsilon \geqslant 10$ in Fig. 2). Note that this effect is not a consequence of the quench in the chain, since it has already been observed in the equilibrium situation $\lambda_i = \lambda_f$ as well. These fast oscillations are directly related to the two high frequencies, proportional to the coupling strength ε, generated by the coupling of the qubits to the chain, whereas the remaining lower frequencies (independent of ε) are responsible for the slower decay of the envelope.

B. Effect of the quench on the Loschmidt echo

We first analyze roughly the effect of the sudden quench dynamics through the evolution of the Loschmidt echo obtained from (23) and (25) by exact numerical diagonalization. Figures 3 and 4 show the time evolution of the Loschmidt echo for several quench protocols for an Ising chain of fixed size $N = 100$, $J = 1$, distance $d = 1$ between qubits, and coupling constants $\varepsilon = 0.1$ and $\varepsilon = 20$, respectively. The first observation that can be made is that the decoherence (and then the disentanglement) is enhanced at long times by the quench in comparison to the unquenched situation (solid lines in Fig. 3 and red curves in Fig. 4), for both the weak and the strong coupling regime. We also note that the higher the quench amplitude $|\lambda_f - \lambda_i|$ becomes, the stronger the disentanglement becomes. This phenomenon is observed numerically whatever the distance between the qubits is. The behavior of the echo with the qubit distance is opposite in the weak and strong coupling regimes: for weak coupling, the echo decreases with the distance, whereas it increases with the distance in the strong coupling regime [25], as shown in Fig. 5, which displays the time evolution of the echo for different distances in the two coupling regimes. Moreover, one observes in the weak coupling regime that the decrease in the Loschmidt echo is monotonous during the time evolution apart for small superimposed oscillations. One can observe beating

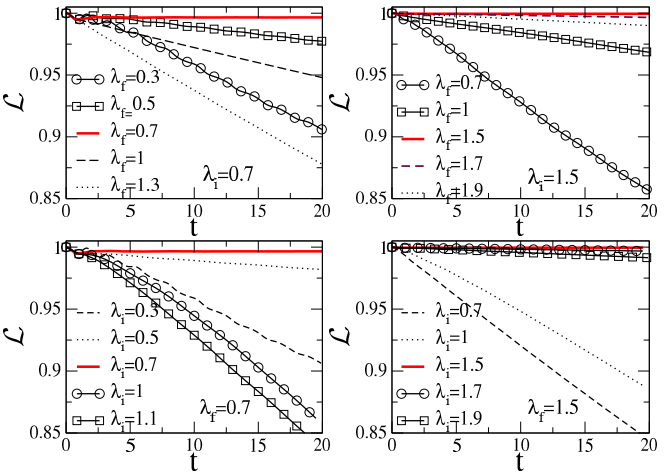

FIG. 3. (Color online) Time evolution of the echo in the weak coupling regime for different quench protocols. For all plots, we choose $N = 100$, $\varepsilon = 0.1$ and keep the distance fixed at $d = 1$. The top two plots are a variation of the final magnetic field, whereas the bottom two plots are a variation of the initial one. For all plots, the varied field is plotted with symbols for $\lambda_i > \lambda_f$, a dashed line for $\lambda_i < \lambda_f$, and a solid line for the equilibrium case $\lambda_i = \lambda_f$.

of the envelope in the strong coupling regime; see, for example, the red curves in Figs. 4(a) and 4(c) . This phenomenon, already observed at equilibrium in [25], can be explained in terms of a decomposition of the spectrum of the Hamiltonian. Indeed, as we mentioned previously, the strong coupling of the qubits to the chain brings two high-frequency excitations of the order of ε, whereas the remaining part of the spectrum can be split into two regions corresponding, respectively, to the region lying between the two qubits and the region lying

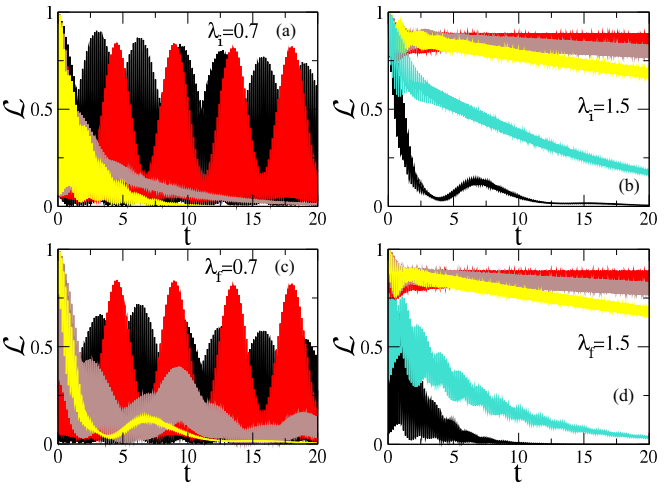

FIG. 4. (Color online) Time evolution of the echo in the strong coupling regime for different quench protocols. For all plots, we choose $N = 100$, $\varepsilon = 20$ and keep the distance fixed at $d = 1$. (a, c) A variation of the final magnetic field; (b, d) a variation of the initial one. In (a) and (c), the varied fields are $\lambda_{i,f} = 0.5$ (black), $\lambda_{i,f} = 0.7$ (red), $\lambda_{i,f} = 1$ (brown), and $\lambda_{i,f} = 1.5$ (yellow). In (b) and (d), the varied fields are $\lambda_{i,f} = 0.7$ (black), $\lambda_{i,f} = 1$ (light blue), $\lambda_{i,f} = 1.5$ (red), $\lambda_{i,f} = 1.7$ (brown), and $\lambda_{i,f} = 1.9$ (yellow).

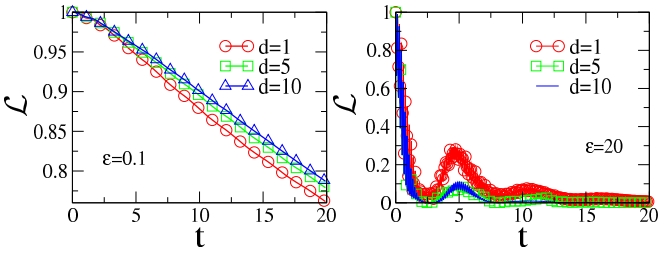

FIG. 5. (Color online) Time evolution of the Loschmidt echo for distances $d = 1$, $d = 5$, and $d = 10$ in the weak (left) and strong (right)coupling regimes. The quench is done from $\lambda_i = 1.5$ to $\lambda_f = 0.5$ and the chain is made of $N = 100$ spins.

outside the interaction sites (this decomposition make sense since $d \ll N$). For fields smaller than the critical field, it turns out that the beating observed in the echo is associated with the lowest energy excitations of the region between the qubits [25]. When the magnetic field increases above the critical value, more and more modes start to be populated, leading to the disappearance of the phenomenon.

In order to characterize the effect of the sudden quench on the disentanglement, we use this monotonic decrease in $\mathcal{L}$ in the weak-coupling regime. We have plotted, in the left panel in Fig. 6, the Loschmidt echo at a fixed, large enough time ($t = 10$) as a function of the initial transverse field value λ_i at two fixed postquench values λ_f (below and above the critical value $\lambda_c = 1$) and, in the right panel, the echo at the same time as a function of the final field at fixed initial fields. We see clearly in these figures that the echo presents a maximum value at the unquenched point (equilibrium situation $\lambda_i = \lambda_f$) showing that the nonequilibrium situation ($\lambda_i \neq \lambda_f$) is always unfavorable with respect to the coherence of the qubits. At the equilibrium point, one recovers the value of $\mathcal{L}$ found in [25]. Away from it, one observes that in the large-field limit the Loschmidt echo saturates at a constant value. This saturation of the decoherence for a high initial magnetic field is easy to understand. Indeed, if λ_i is very large, the initial state is close to a completely polarized state along the direction of the field $|\Psi\rangle = |\uparrow\uparrow \ldots \uparrow\rangle$. In this limiting case, the initial covariance matrix is trivially

$$C(0) = \begin{pmatrix} \mathbb{1} & 0 \\ 0 & 0 \end{pmatrix} \tag{27}$$

and obviously no longer depends on the initial magnetic field λ_i, and consequently, neither does the Loschmidt echo. In the left panel in Fig. 6 the saturation value of the echo for a completely polarized initial state is shown by dashed lines for the two final fields considered there. We see that the Loschmidt echo converges asymptotically to these limiting values. In the right panel in Fig. 6, one sees that the same saturation phenomenon applies with respect to large final fields.

The Loschmidt echo, and subsequently the entanglement, exhibits a signature of the quantum phase transition experienced by the Ising chain. Indeed, when the initial magnetic field is varied, we clearly see a jump in the curve for λ_i close to the critical value $\lambda_c = 1$. This critical behavior is better seen by analyzing the first derivative of $\mathcal{L}(t)$ with respect to the

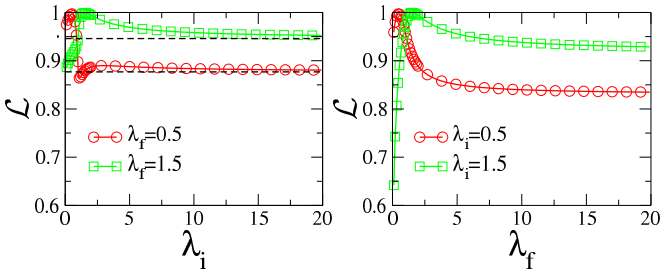

FIG. 6. (Color online) Loschmidt echo at time $t = 10$ as a function of the initial (final fixed; left) and final (initial fixed; right) magnetic field. The varied magnetic fields are 0.5 [(red) circles] and 1.5 [(green) squares]. Dashed lines represent the limiting case of a completely polarized initial state ($J = 0$).

initial field λ_i. The derivative with respect to the initial field, at fixed time $t = 10$, is plotted in Fig. 7 for final fields in the ordered ($\lambda_f = 0.5$) and disordered ($\lambda_f = 1.5$) phases. For the two cases, the first derivative exhibits a clear singularity when the bath approaches criticality. Note that, on one hand, the derivative is negative for $\lambda_f = 0.5$, reflecting the fact that the divergence occurs after the equilibrium point ($\lambda_f = \lambda_i = 0.5$) when the echo is decreasing with the field. On the other hand, it is positive at $\lambda_f = 1.5$, since the divergence occurs before the equilibrium point ($\lambda_f = \lambda_i = 1.5$) when the echo is increasing with the field. On the other hand, there is no clear signature of a singularity, as shown in the inset in Fig. 7, with respect to a variation of the final field for fixed initial fields $\lambda_i = 0.5$ and $\lambda_i = 1.5$. This indicates that the critical behavior is totally set by the initial state of the environment, whereas the final magnetic field is only responsible for dynamical effects, as we see later.

Due to the finite size of the environment, the singularity of the absolute value of the first derivative of the Loschmidt

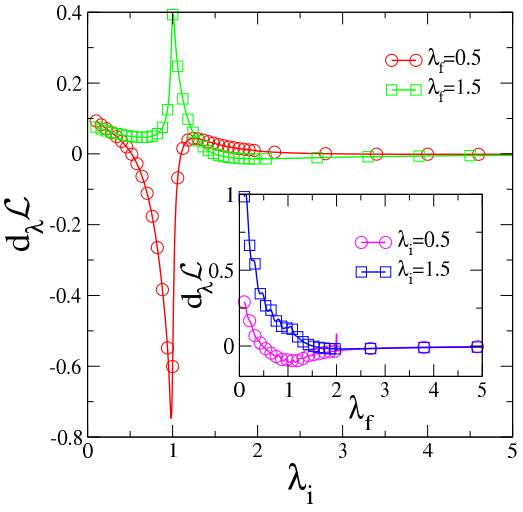

FIG. 7. (Color online) First derivative of the Loschmidt echo at time $t = 10$ as a function of the initial magnetic field for $\lambda_f = 0.5$ [(red) circles] and $\lambda_f = 1.5$ [(green) squares]. Other parameters are $\varepsilon = 0.1$, $d = 1$, and $N = 100$. Inset: The derivative of $\mathcal{L}$ with respect to the final field λ_f for $\lambda_i = 0.5$ [(magenta) circles] and $\lambda_i = 1.5$ [(blue) squares].

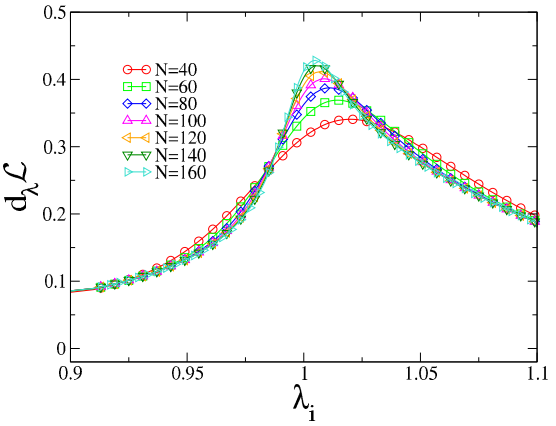

FIG. 8. (Color online) First derivative of the Loschmidt echo at time $t = 10$ as a function of the initial magnetic field for different sizes of the bath with $\lambda_f = 1.5$, $\varepsilon = 0.1$, and $d = 1$.

echo is rounded and reaches a maximum value at a given $\lambda_{\max}$ of the initial field (see Fig. 8). As the size of the environment increases, the maximum value of $|d_\lambda \mathcal{L}|$ diverges logarithmically with the size $d_\lambda \mathcal{L}|_{\lambda_{\max}} \sim \ln N$. At the same time the value $\lambda_{\max}$ of the initial field approaches asymptotically the critical value $\lambda_c = 1$ as $|\lambda_c - \lambda_{\max}| \sim N^\gamma$ with an exponent γ which is found numerically to be ~ -1.1, as shown in Fig. 9. The expected value from critical scaling theory [41] is $\gamma = -1/\nu = -1$, since the correlation length exponent $\nu = 1$ for the quantum Ising chain. The departure from that value is due to the quite strong corrections to scaling and is numerically compatible with a scaling correction $N(\lambda_c - \lambda_{\max}) \sim 1 + \text{const.}/N$. Note that these scaling results are comparable to those found in Refs. [15,42].

C. Short-time behavior

For times much shorter than the typical time scale of the system $t \ll t_{\text{typ}}$ with

$$t_{\text{typ}} = 1 \quad \text{for} \quad \varepsilon \ll 1, \tag{28}$$

$$t_{\text{typ}} = 1/\varepsilon \quad \text{for} \quad \varepsilon \gg 1, \tag{29}$$

the Loschmidt echo shows a parabolic decay independent of the quench parameters as shown in Fig. 10.This independence is easily understood from a perturbative approach [43]. Indeed, expanding the ground state $|G(\lambda_i)\rangle$ in the eigenbasis $\{|\phi_m\rangle\}$ and

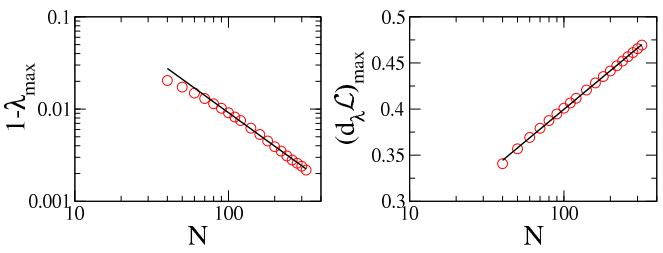

FIG. 9. (Color online) Left: Scaling behavior of the position of the peaks $\lambda_{\max}$ as a function of the size of the bath N. Right: Scaling behavior of the maximum value reached by $d_\lambda \mathcal{L}$ as a function of the size of the bath N. Parameters are $\lambda_f = 1.5$, $\varepsilon = 0.1$, and $d = 1$.

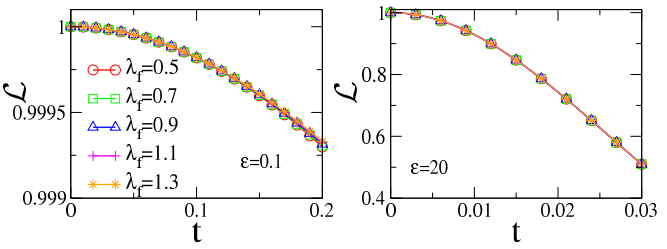

FIG. 10. (Color online) Short-time evolution of the Loschmidt echo for different values of the final field and $\varepsilon = 0.1$ (left) and $\varepsilon = 20$ (right). Other parameters are $\lambda_i = 0.7$ and $N = 100$.

$\{|\varphi_m\rangle\}$ of $H_{\downarrow\downarrow}$ and $H_{\uparrow\uparrow}$, respectively, $|G(\lambda_i)\rangle = \sum_m a_m|\phi_m\rangle = \sum_m b_m|\varphi_m\rangle$, the echo becomes

$$\mathcal{L}(t) = \left|\sum_{mn} a_m^* b_n e^{-i(E_n^{\uparrow\uparrow} - E_m^{\downarrow\downarrow})t}\langle\phi_m|\varphi_n\rangle\right|^2. \tag{30}$$

At first order in perturbation theory, the eigenvalues are given by

$$E_n^{\uparrow\uparrow} = E_n^{\downarrow\downarrow} + \langle\phi_n|\tilde{H}_I|\phi_n\rangle = E_n^{\downarrow\downarrow} + V_n, \tag{31}$$

where $\tilde{H}_I = -\varepsilon(\sigma_0^z + \sigma_d^z)$. If the interaction Hamiltonian is sufficiently small, the decomposition coefficients $a_m \approx b_m$ and $\langle\phi_m|\varphi_n\rangle \approx \delta_{m,n}$ such that

$$\mathcal{L}(t) \approx \left|\sum_n |a_n|^2 e^{-iV_n t}\right|^2. \tag{32}$$

Expanding the exponential up to second order in time, one obtains

$$\begin{aligned}\mathcal{L}(t) &\approx \left|\sum_m |a_m|^2\left(1 - itV_m - \frac{t^2}{2}(V_m)^2\right)\right|^2 \\ &\approx 1 - \left(\sum_m |a_m|^2 V_m^2 - \left(\sum_m |a_m|^2 V_m\right)^2\right)t^2 \\ &\approx 1 - \left(\langle\tilde{H}_I^2\rangle - \langle\tilde{H}_I\rangle^2\right)t^2 \equiv 1 - \alpha t^2.\end{aligned} \tag{33}$$

Then, for short times, the echo depends only on the variance of the interaction Hamiltonian over the initial state $|G(\lambda_i)\rangle$ and, consequently, not on the quench protocol itself.

The Gaussian rate (the variance) α is easily evaluated by expressing $\tilde{H}_I$ in terms of the normal modes of the Hamiltonian $H_E(\lambda_i)$:

$$\begin{aligned}\tilde{H}_I = -2\varepsilon \sum_{kl}[&(g_{0k}\eta_k^\dagger + h_{0k}\eta_k)(g_{0l}\eta_l + h_{0l}\eta_l^\dagger) \\ &+ (g_{dk}\eta_k^\dagger + h_{dk}\eta_k)(g_{dl}\eta_l + h_{dl}\eta_l^\dagger)] + 2\varepsilon.\end{aligned} \tag{34}$$

Using the fact that $\langle\eta_k\eta_l\rangle = \langle\eta_k^\dagger\eta_l^\dagger\rangle = 0$ and $\langle\eta_k\eta_l^\dagger\rangle = \delta_{kl}$, the variance α is expressed as

$$\begin{aligned}\alpha = 4\varepsilon^2 \sum_{k\neq l}[&(g_{0k}h_{0l} + g_{dk}h_{dl})^2 - 2h_{dk}h_{0l}g_{dl}g_{0k} \\ &- h_{0k}h_{0l}g_{0k}g_{0k} - h_{dk}h_{dl}g_{dk}g_{dk}].\end{aligned} \tag{35}$$

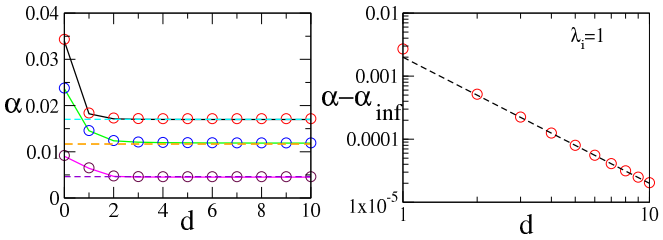

FIG. 11. (Color online) Gaussian rate α as a function of the parameters of the system. Left: α as a function of the distance d for a final field $\lambda_f = 0.5$ and, from top to bottom, $\lambda_i = 0.7$, $\lambda_i = 1$, and $\lambda_i = 1.5$. Circles are the numerical fits of the echo, solid lines are obtained with Eq. (35), and dashed horizontal lines give the asymptotic ($d \to \infty$) values of α. Right: $\alpha - \alpha_{d\to\infty}$ in the critical case $\lambda_i = 1$ and for $\lambda_f = 0.5$ as a function of the distance d, showing a power-law behavior with exponent -2, shown by the dashed curve.

Note that α is nothing but $2\varepsilon^2(\langle\sigma_0^z\sigma_d^z\rangle_c + 1 - \langle\sigma_0^z\rangle^2)$, where $\langle AB\rangle_c \equiv \langle AB\rangle - \langle A\rangle\langle B\rangle$ is the connected correlation function [47]. In particular, at large distances compared to the correlation length ξ in the initial ground state, i.e., $d \gg \xi$, since $\langle\sigma_0^z\sigma_d^z\rangle_c = 0$, one expects a saturation value $\alpha(d \gg 1) = 2\varepsilon^2(1 - \langle\sigma_0^z\rangle^2)$. However, when the initial state is critical, that is, for $\lambda_i = 1$, since the decay of the connected part is algebraic with $\langle\sigma_0^z\sigma_d^z\rangle_c \sim d^{-2}$ [41], the approach toward the saturation value $\alpha(d \to \infty)$ is algebraic, as shown in Fig. 11.When the initial-state field λ_i is close enough to the critical point $\lambda_i = 1$, the first derivative of α, $d_{\lambda_i}\alpha$, exhibits a logarithmic divergence typical from the two-dimensional Ising universality class.

In Fig. 10, we show the short-time evolution of the Loschmidt echo for different quench protocols in both the weak and the strong regimes. We see that it does not depend on the value of the final magnetic field λ_f for times $t < t_{\rm typ}$ as expected from (33) and observed in [21].

Figure 11 shows the dependence of the Gaussian rate α as a function of d for different quench protocols in the weak coupling case.

D. Revival times

In the preceding section we have considered the short-time behavior of the system, which is shorter than a revival time. However, depending on the separation distance d and on the system size N we observe a significant change in the Loschmidt echo for times of the order N. Note that this behavior is shown in the weak coupling case only, but the same phenomenon is also observed in the strong coupling regime. For times $1 \lesssim t < N/4$, when the initial state is not critical we observe a linear decay of the echo whatever the final field is. This is shown in Fig. 12 for systems of total size $N = 100$ and $N = 200$. We see, in particular, that when the separation distance of the two qubits is far from the symmetric opposite position (that is, $d = N/2$), the initial linear decay reverts to a linear increase at a revival time $t^* \simeq N/4$. The increase in the echo switches again to a linear decay after $t \simeq 2t^* \simeq 2 \times N/4$, and so on.

When the separation distance d comes close to the opposite location $N/2$, we observe a new singularity, emerging at half the original revival time, setting a new time scale, $\tau^* \simeq t^*/2 \simeq N/8$. This new time scale τ^* is manifesting itself

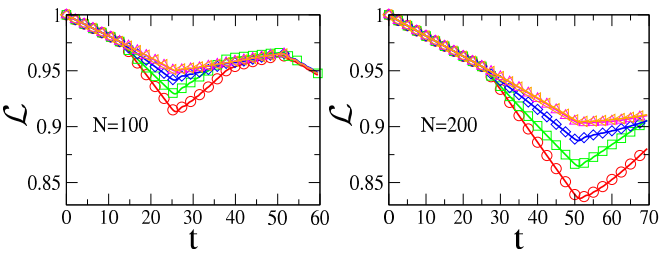

FIG. 12. (Color online) Loschmidt echo for distances $d = N/2$ [(red) circles], $d = N/2 - 1$ [(green) squares], $d = N/2 - 2$ [(blue) diamonds], $d = N/2 - 5$ [(magenta) upward triangles], and $d = N/2 - 15$ [(orange) leftward triangles] for $N = 100$ (left) and $N = 200$ (right). Note that due to their almost-perfect matching, the two curves for $d = N/2 - 5$ and $d = N/2 - 15$ are not distinguishable. Other parameters are set to $\varepsilon = 0.1$, $\lambda_i = 1.5$, and λ_f=0.99.

in a sudden speedup of the linear decay until the revival time t^* is reached. The maximum slope of the new regime is reached when the two qubits sit exactly on opposite sites along the chain, that is, for $d = N/2$. This is best shown in the left panel in Fig. 13, which shows the numerical derivative of the echo for distances $d = N/2, N/2 - 1, N/2 - 2, N/2 - 5$, and $N/2 - 15$. One observes, in particular, that the new time scale τ^* has disappeared already for $d = N/2 - 5$ (see Fig. 12). Note the remarkable feature that, whatever distance d is, at time $t = 2t^*$ the Loschmidt echo recovers approximately the same value, as clearly shown in the left panel in Fig. 12.

In the right panel in Fig. 13 we have plotted the evolution of the echo for two qubits at a distance $d = 1$ for several quench protocols including the equilibrium situation $\lambda_i = \lambda_f$. We see that, contrary to the opposite location ($d = N/2$) situation, there is no effect at $t = \tau^*$. One observes the revival phenomenon occurring at $t^* \simeq N/4$ for the two nonequilibrium quenches considered here ($\lambda_i = 0.7$, 0.9 to $\lambda_f = 0.99$). However, one clearly notes that in the equilibrium situation ($\lambda_i = \lambda_f$) the revival occurs at a time $t^*_{\rm eq}$ which is twice the nonequilibrium revival time t^*.

The fact that the revival time is twice as short in the nonequilibrium quench case ($\lambda_i \neq \lambda_f$) as in the equilibrium situation ($\lambda_i = \lambda_f$) can be understood in the following way [44]: Indeed, the nonequilibrium situation corresponds to a global quench. At each position of the chain the energy is suddenly changed

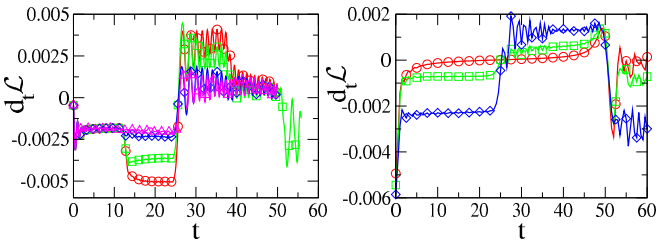

FIG. 13. (Color online) First derivative of the Loschmidt echo with respect to time. Left: $\lambda_i = 1.5$ and $\lambda_f = 0.99$ are kept fixed, and the distance is varied. $d = N/2$ [(red) circles], $d = N/2 - 1$ [(green) squares], $d = N/2 - 2$ [(blue) diamonds], and $d = N/2 - 15$ [(magenta) triangles]. Right: The distance is $d = 1$, and $\lambda_f = 0.99$ and $\lambda_i = 0.99$ [(red) circles], $\lambda_i = 0.9$ [(green) squares], and $\lambda_i = 0.7$ [(blue) diamonds]. Other parameters are $\varepsilon = 0.1$ and $N = 100$.

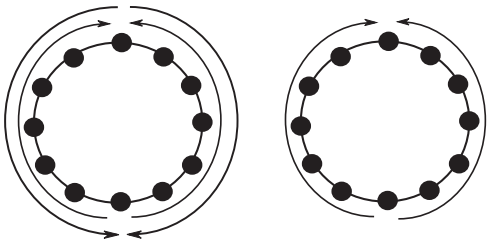

FIG. 14. Pictorial representation of the difference between the global quench (left) and the local quench (equilibrium; right). In the quenched case, excitations are emitted from everywhere, in particular, in one spin and its opposite. Then the revival time is the time required for the excitations to travel a distance which is half the chain length. On the contrary, in the equilibrium situation, excitations are emitted in only one position, and the revival time is the time needed to travel along the entire chain.

and from every point pairs of free quasiparticles are emitted with opposite momenta $\pm k$. The fastest particles travel at velocities

$$v_g = \max_k \left(\frac{\partial \varepsilon_k}{\partial k} \right) \Big|_k = \begin{cases} 2\lambda_f & \text{if} \quad \lambda_f < 1, \\ 2 & \text{if} \quad \lambda_f \geqslant 1, \end{cases} \tag{36}$$

and since all chain sites behave as local emitters after a time $t^* = \frac{1}{2} N/v_g$ the configuration of quasiparticles along the chain is starting to restore its initial state, leading to the increase in the echo. On the contrary, the equilibrium case corresponds to a local quench at the qubits' positions. In this case, quasiparticles are emitted only at that localized site and they need to circle at least once along the full chain to reconstruct the initial state, such that $t^* = N/v_g$. This quasiparticle interpretation is depicted schematically in Fig. 14.

When the starting state is long-range, that is, for an initial field value λ_i very close to the critical value $\lambda_c = 1$, the revival phenomenology is very similar to what has already been discussed: At symmetric positions of the defect qubits ($d \simeq N/2$), one observes a singular behavior of the echo at time $\tau^* = t^*/2$ and a revival phenomenon starting at t^*. Far from the symmetric position, the singular behavior at τ^* has disappeared and just the revival time t^* shows up. For the nonequilibrium quench ($\lambda_i \neq \lambda_f$) the revival time $t^* = N/4$, while for the equilibrium case ($\lambda_i = \lambda_f$) the revival time $t^* = N/2$ is twice as long. The main difference from the noncritical initial state lies in the fact that the shape of the decay (and increase) of the Loschmidt echo is no longer linear as it was for the initial short-range state (see Fig. 15).

E. Comparison to the independent dynamics

Part of the disentanglement observed between the two qubits is a consequence of their direct coupling to the environment, and the other part comes from their mutual interaction, mediated through the bath degrees of freedom. In order to quantify the part of the decoherence that comes from this direct coupling we compute the difference in the Loschmidt echo between the situation where the spins are coupled to a common environment and the limiting case of two spins coupled to two independent ones: $\Delta\mathcal{L} = \mathcal{L} - \mathcal{L}_{\text{ind}}$. The results are presented in Fig. 16, where we have plotted

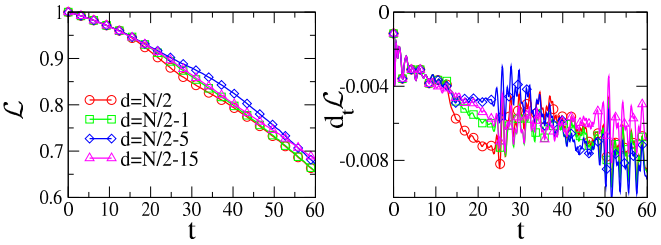

FIG. 15. (Color online) Left: Loschmidt echo for a critical initial environment for distances $d = N/2$ [(red) circles], $d = N/2 - 1$ [(green) squares], $d = N/2 - 5$ [(blue) diamonds], and $d = N/2 - 15$ [(magenta) triangles]. Right: Time derivative of the Loschmidt echo for the previous distances. Other parameters are $N = 100$, $\lambda_f = 1.5$, and $\varepsilon = 0.1$.

$\Delta\mathcal{L}$ as a function of time for different quench protocols and distances d.

For initial magnetic fields far enough from the critical field, the difference $\Delta\mathcal{L}$ is equal to 0 up to a time t_{ind} after which $\mathcal{L}$ and $\mathcal{L}_{\text{ind}}$ starts to differ significantly. This implies that for times shorter than t_{ind}, the two spins are evolving independently as if they were coupled to a noninteracting bath. After t_{ind}, the two spins start to interact through the chain and their evolution is no longer independent. Note that this time is not dependent on the initial magnetic fields but, rather, depends on the final one and, of course, on the distance between the two defect spins. This can be understood in the following way: the two spins will evolve independently until an entangled pair of excitations created by the quench in the middle of the two qubits has reached them and consequently correlated them. The time required for this pair of excitations to travel along the chain is given by $t_{\text{ind}} = (d/2)/v_g$, where the velocity v_g is given by (36) and depends only on λ_f. Note that in the equilibrium situation, the fact that the quasiexcitations are emitted at positions 0 and

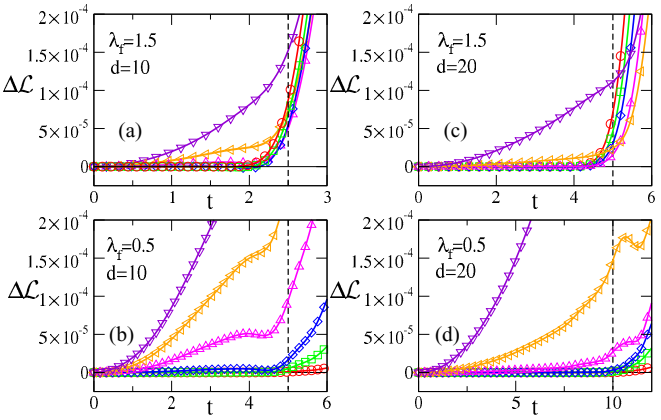

FIG. 16. (Color online) Difference in the Loschmidt echo $\Delta\mathcal{L}$ in the situation where the two spins are coupled to the same bath versus to two independent baths as a function of time for different quench protocols and distances. Initial magnetic fields are $\lambda_i = 0.4$ [(red) circles in (b) and (d)], $\lambda_i = 0.5$ [(red) circles in (a) and (c)], $\lambda_i = 0.7$ [(green) squares], $\lambda_i = 0.8$ [(blue) diamonds], $\lambda_i = 0.9$ [(magenta) upward triangles], $\lambda_i = 0.95$ [(orange) leftward triangles], and $\lambda_i = 1$ [(indigo) downward triangles]. In all plots, the vertical dashed line represents the theoretical value of $t_{\text{ind}} = d/(2v_g)$.

d leads to a twice bigger $t_{\rm ind}$. The time $t_{\rm ind}$ is indicated in Fig. 16 by the dashed vertical lines. We see that this prediction is in quite good agreement with the numerical data.

On the other hand, when the initial magnetic field is close to the critical value $\lambda_i = 1$, there is already a nonvanishing difference $\Delta\mathcal{L}$ at $t = 0^+$ due to the long-range correlations present in the chain. The typical correlation length in the Ising chain is given by $\xi = |\ln(\lambda_i)|^{-1}$ [45], and if the distance d separating the two defect qubits is smaller than this correlation length ξ, the two defects are no longer independent already at $t = 0$. This is clearly shown in Fig. 16 for $\lambda_i = 0.95$ and 1, where we see the large departure of $\Delta\mathcal{L}$ from 0. Moreover, at a fixed initial field λ_i (that is, at a fixed correlation length ξ), the larger the separation distance d between the two defect spins, the smaller the departure from 0 of $\Delta\mathcal{L}$, as seen by comparing Figs. 16(a) and 16(b), where the distance was fixed at $d = 10$, to Figs. 16(c) and 16(d), where $d = 20$. Nevertheless, the signature of the correlation of the qubits through the entangled pair emission mechanism, discussed above for short-range initial states, is also present in this critical case. We observe clearly in Fig. 16 a significant deviation of $\mathcal{L}$ to $\mathcal{L}_{\rm ind}$ for times longer than $t_{\rm ind}$.

V. CONCLUSION AND SUMMARY

We have investigated the effect on the disentanglement of two qubits initially prepared in a Bell state of a global quench of an Ising chain environment to which the qubits are coupled. We have, in particular, studied the dependence of the decoherence on the distance separating the two qubits. We have shown that the decoherence of the qubits is enhanced at long times in the quenched environment case with respect to the equilibrium chain considered in [25]. We have seen that the higher the quench amplitude, the stronger the decoherence, such that the quenched situation always leads to an increased qubit decoherence. When the initial state of the Ising chain environment is close to criticality the Loschmidt echo exhibits a clear signature of the long-range nature of the initial state. At long times, of the order of the environment size (the number of sites N of the ITF), we observe a revival phenomenology in the Loschmidt echo starting at a time t^* which is twice as short as that in the equilibrium case. This is explained in terms of the propagation of quasiparticles emitted, due to the global quench, at every site of the ITF chain, contrary to the equilibrium situation, where only sites directly coupled to the two qubits act as quasiparticle emitters. As a consequence of the propagation of the quasiparticles in the chain, they have to travel half the chain length in order to rebuild the initial correlations, while they have to circle around the full chain in order to start to rebuild correlations in the equilibrium case. Finally, one observes an intriguing phenomenon when the qubits are coupled on opposite sites of the ITF chain, that is, when they are maximally separated; indeed, there is singular behavior appearing in the Loschmidt echo at half the revival time scale, t^*, which does not seem to be explainable in terms of quasiparticle propagation but, rather, is an interference effect.

ACKNOWLEDGMENTS

We are grateful to Giovanna Morigi and Cecilia Cormick for helpful discussions. P.W. benefited from the support of the International Graduate College on Statistical Physics of Complex Systems, among the universities of Lorraine, Leipzig, Coventry, and Lviv.

[1] R. Horodecki, P. Horodecki, M. Horodecki, and K. Horodecki, Rev. Mod. Phys. **81**, 865 (2009).
[2] A. Einstein, B. Podolsky, and N. Rosen, Phys. Rev. **47**, 777 (1935).
[3] B. Berche, C. Chatelain, C. Dufour, T. Gourieux, and D. Karevski, Cond. Mat. Phys. **9**, 319 (2006).
[4] M. A. Nielsen and I. L. Chuang, *Quantum Computation and Quantum Information* (Cambridge University Press, Cambridge, 2000).
[5] I. Georgescu, S. Ashhab, and F. Nori, Rev. Mod. Phys. **86**, 153 (2014).
[6] J. P. Paz and W. H. Zurek, in *Coherent Atomic Matter Waves* (Springer, Berlin, 2001), p. 533.
[7] W. H. Zurek, Los Alamos Science **27**, 86 (2002).
[8] M. A. Schlosshauer, *Decoherence: And the Quantum-to-Classical transition* (Springer, Berlin, 2007).
[9] L. Viola and S. Lloyd, Phys. Rev. A **58**, 2733 (1998).
[10] D. Rossini, P. Facchi, R. Fazio, G. Florio, D. A. Lidar, S. Pascazio, F. Plastina, and P. Zanardi, Phys. Rev. A **77**, 052112 (2008).
[11] T. Fogarty, E. Kajari, B. G. Taketani, A. Wolf, T. Busch, and G. Morigi, Phys. Rev. A **87**, 050304 (2013).
[12] B. G. Taketani, T. Fogarty, E. Kajari, T. Busch, and G. Morigi, Phys. Rev. A **90**, 012312 (2014).
[13] G. Goldstein, P. Cappellaro, J. R. Maze, J. S. Hodges, L. Jiang, A. S. Sørensen, and M. D. Lukin, Phys. Rev. Lett. **106**, 140502 (2011).
[14] L. Cincio, J. Dziarmaga, M. M. Rams, and W. H. Zurek, Phys. Rev. A **75**, 052321 (2007).
[15] A. Osterloh, L. Amico, G. Falci, and R. Fazio, Nature **416**, 608 (2002).
[16] F. M. Cucchietti, J. P. Paz, and W. H. Zurek, Phys. Rev. A **72**, 052113 (2005).
[17] H. T. Quan, Z. Song, X. F. Liu, P. Zanardi, and C. P. Sun, Phys. Rev. Lett. **96**, 140604 (2006).
[18] F. M. Cucchietti, S. Fernandez-Vidal, and J. P. Paz, Phys. Rev. A **75**, 032337 (2007).
[19] Z.-G. Yuan, P. Zhang, and S.-S. Li, Phys. Rev. A **76**, 042118 (2007).
[20] B. Damski, H. T. Quan, and W. H. Zurek, Phys. Rev. A **83**, 062104 (2011).
[21] V. Mukherjee, S. Sharma, and A. Dutta, Phys. Rev. B **86**, 020301 (2012).
[22] S. Sharma, V. Mukherjee, and A. Dutta, Eur. Phys. J. B **85**, 1 (2012).
[23] T. Nag, U. Divakaran, and A. Dutta, Phys. Rev. B **86**, 020401 (2012).
[24] A. Faribault and D. Schuricht, Phys. Rev. B **88**, 085323 (2013).

[25] C. Cormick and J. P. Paz, Phys. Rev. A **78**, 012357 (2008).
[26] P. Calabrese and J. Cardy, J. Stat. Mech.: Theor. Exp. (2007) P06008.
[27] A. Polkovnikov, K. Sengupta, A. Silva, and M. Vengalattore, Rev. Mod. Phys. **83**, 863 (2011).
[28] S. Dorosz, T. Platini, and D. Karevski, Phys. Rev. E **77**, 051120 (2008).
[29] D. Karevski, Eur. Phys. J. B **27**, 147 (2002).
[30] V. Hunyadi, Z. Rácz, and L. Sasvári, Phys. Rev. E **69**, 066103 (2004).
[31] T. Platini and D. Karevski, Eur. Phys. J. B **48**, 225 (2005).
[32] T. Platini and D. Karevski, J. Phys. A: Math. Theor. **40**, 1711 (2007).
[33] M. Collura and D. Karevski, Phys. Rev. Lett. **104**, 200601 (2010).
[34] M. Collura and D. Karevski, Phys. Rev. A **83**, 023603 (2011).
[35] M. Collura, H. Aufderheide, G. Roux, and D. Karevski, Phys. Rev. A **86**, 013615 (2012).
[36] P. Wendenbaum, M. Collura, and D. Karevski, Phys. Rev. A **87**, 023624 (2013).
[37] A. Goussev, R. A. Jalabert, H. M. Pastawski, and D. A. Wisniacki, Scholarpedia **7**, 11687 (2012).
[38] W. K. Wootters, Phys. Rev. Lett. **80**, 2245 (1998).
[39] W. K. Wootters, Quant. Inf. Comp. **1**, 27 (2001).
[40] M. Keyl and D.-M. Schlingemann, J. Math. Phys. **51**, 023522 (2010).
[41] M. Henkel, *Conformal Invariance and Critical Phenomena* (Springer, Berlin, 1999).
[42] H.-Q. Zhou, J.-H. Zhao, and B. Li, J. Phys. A: Math. Theor. **41**, 492002 (2008).
[43] A. Peres, Phys. Rev. A **30**, 1610 (1984).
[44] P. Calabrese and J. Cardy, J. Stat. Mech.: Theor. Exp. (2005) P04010.
[45] P. Pfeuty, Ann. Phys. **57**, 79 (1970).
[46] D. Rossini, T. Calarco, V. Giovannetti, S. Montangero, and R. Fazio, Phys. Rev. A **75**, 032333 (2007).
[47] Note, also, that if we set $d = 0$ in this expression (the two spins are coupled at the same site), we recover the formula obtained in [46], but with a coupling constant two times stronger since $\tilde{H}_I = -\varepsilon(\sigma_0^z + \sigma_{d=0}^z) = -(2\varepsilon)\sigma_0^z$.